Research Article Vol. 56, No. 20 / July 10 2017 / Applied Optics 5781

Asymmetric transmission of obliquely intersecting nanoslit arrays in a gold film

YUYAN CHEN, YONGKAI WANG, TIANKUN WANG, YONGYUAN ZHANG, LI WANG, AND ZHONGYUE ZHANG*

School of Physics and Information Technology, Shaanxi Normal University, Xi'an 710062, China
**Corresponding author: zyzhang@snnu.edu.cn*

Received 13 April 2017; revised 14 June 2017; accepted 20 June 2017; posted 21 June 2017 (Doc. ID 292800); published 10 July 2017

Asymmetric transmission (AT) has significant applications in optical polarization control. In this paper, we propose a kind of periodic nanoslit rather than the protruding planar structures, such as G-shaped structure and coupled split-ring resonators, to realize the AT effect. The planar periodic obliquely intersecting nanoslits (OINs) in the gold film, composed of gratings with an infinite length and tilted nanoslits with a finite length, are proposed to realize the AT effect by performing the finite element method. Obvious dips in the AT spectra result from the circular localized surface plasmon resonance around the two terminals of the tilted nanoslits and from the surface plasmon polariton resonances on the film and in the gratings or tilted nanoslits. In addition, the AT effect strongly depends on the geometric parameters of the OINs. The film can be straightly powered on as an in-plane electrical conductor, which broadens its applications in optoelectronic devices. Overall, these results are beneficial in designing devices to achieve AT for polarization transformation.

OCIS codes: (250.5403) Plasmonics; (260.5430) Polarization; (160.4236) Nanomaterials; (230.5440) Polarization-selective devices.

https://doi.org/10.1364/AO.56.005781

1. INTRODUCTION

During the past several years, many interesting electromagnetic properties have been shown in chiral metamaterial, such as circular dichroism [1–3], negative refractive index [4–6], and asymmetric transmission (AT) effect [7–10]. The AT effect was found for the first time in metamaterial by Fedotov *et al.* [11]. Their study indicated that the AT effect is related not only to the direction of wave propagation but also to the polarization states of incident waves. In consideration of the strong interaction between electromagnetic waves and chiral metal structures, AT is a consequence of acquiring different polarization state waves from illuminating the same polarization state waves in opposite directions [12–15]. This interesting phenomenon is widely applicable in the design of polarization transformers and optical devices [16–18].

At present, many complex 3D structures have been studied to generate the AT effect upon excitation of circularly polarized waves. The AT effect of helical plasmonic nanostructures is a consequence of introducing spatial asymmetry in helical chiral nanostructures [19,20]. Moreover, layer-by-layer structures have been introduced to produce the AT effect from electromagnetic coupling between adjacent layers [21–23]. Preparing helical or multilayer chiral metamaterials by bottom-up and top-down fabrication technologies leads to a complicated process [24]. Therefore, planar structures generating the AT effect, such as G-shaped structure, coupled split-ring resonators, and chiral fish scale structure, have become research hotspots [25–27]. The planar structure is easier to fabricate than multilayer structures, and metal films with nanoslits can confine localized electric fields along the nanoslits. Thus, designing nanoslits in a film could help elucidate the mechanism behind the AT effect and could exhibit promising applications.

In this paper, we propose planar obliquely intersecting nanoslit (OIN) arrays in a gold film to generate the AT effect. The OINs consist of gratings with an infinite length and tilted nanoslits with a finite length. Calculation results from the finite element method show that strong AT signals occur around resonance wavelengths. The AT effect arises from the different responses of the circular localized surface plasmon (LSP) resonances around the two terminals of the tilted nanoslits or the surface plasmon polariton (SPP) on the film and in the gratings or tilted nanoslits under excitation by different polarized lights. In addition, the AT effect is related to the geometric parameters of the OINs, such as the angle between the gratings and tilted nanoslits, the widths of the gratings and tilted nanoslits, the thickness of the OINs, and the periods of the OINs. The OIN arrays are easy to fabricate, and, compared to the protruding planar structures, such as G-shaped structure and coupled split-ring resonators, OIN arrays can be directly powered on as specific electrodes, which broadens its applications in polarization and optoelectronic devices [28–30].

2. STRUCTURE AND COMPUTATIONAL METHOD

Figure 1 shows the schematic and the geometric parameters of the OIN arrays in the gold film. The dielectric function of gold is obtained from the experimental data of Johnson and Christy [31]. Lights transmit in the $-z$ direction as shown in Fig. 1(a). The unit is presented in Fig. 1(b) with periods P_x and P_y in the $x-y$ plane. The thickness of the film is t. The single grating has a width of w_0. The single tilted nanoslit has a width of w and a length of l. The angle between gratings and tilted nanoslits is β.

In the study, the transmission spectra and AT spectra are achieved using the 3D finite element method with software COMSOL Multiphysics. There are two perfectly matched layers whose purpose is to decrease the reflection to zero, located at the bottom and top of the whole structure, respectively. In order to build infinite periodic arrays of the OINs in space, two series of periodic conditions have been set along the x direction and y direction, respectively. The minimum mesh size of OINs is set as 0.9 nm, which satisfies the COMSOL stability criteria.

The total transmission coefficient is defined as T_{+}^{+z} (T_{-}^{-z}), where the superscript indicates the propagation of incident waves along $+z$ ($-z$) direction, and the subscript "+" ("−") indicates right circularly polarized (RCP) waves [left circularly polarized (LCP) waves]. For the RCP incident waves propagating along $-z$ direction, T_{-+}^{-z} and T_{++}^{-z} represent transmission coefficients of transmitted LCP waves and transmitted RCP waves, respectively. Similarly, the same principle applies to LCP incident waves propagating along $-z$ direction. There are two parts existing in the transmitted waves when one state of the circularly polarized wave is incident, so the total transmission of one polarization state can be described as

$$T_{+}^{+z} = T_{++}^{+z} + T_{-+}^{+z}, \quad T_{+}^{-z} = T_{++}^{-z} + T_{-+}^{-z}. \tag{1}$$

Thus, the AT effect can be described as

$$\mathrm{AT} = T_{+}^{+z} - T_{+}^{-z} = (T_{++}^{+z} + T_{-+}^{+z}) - (T_{++}^{-z} + T_{-+}^{-z}). \tag{2}$$

While the Lorentz Reciprocity Theorem requires $T_{++}^{+z} = T_{++}^{-z}$, $T_{-+}^{+z} = T_{+-}^{-z}$ [32], then AT can be deduced as

$$\mathrm{AT}^{-z} = T_{-+}^{+z} - T_{-+}^{-z} = T_{+-}^{-z} - T_{-+}^{-z} = -\mathrm{AT}^{+z}. \tag{3}$$

Equation (3) means that the value of AT under excited circularly polarized lights along $-z$ direction is opposite to that of $+z$ direction. For clear and concise expression, we discuss only the condition of circularly polarized light illuminating along $-z$ direction.

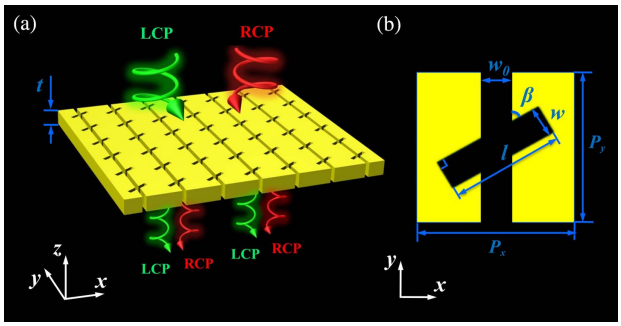

Fig. 1. (a) Schematic of OIN arrays in the gold film with $P_x = P_y = 500$ nm, $t = 200$ nm, $w = 50$ nm, $w_0 = 50$ nm, $l = 300$ nm, and $\beta = 60°$. (b) Its unit cell with the associated parameters definition.

3. RESULTS AND DISCUSSION

Figure 2(a) shows the transmission spectra of the OINs under circularly polarized excitation with the following parameters: $P_x = P_y = 500$ nm, $t = 200$ nm, $w_0 = w = 50$ nm, $l = 300$ nm, and $\beta = 60°$. Three obvious peaks at $\lambda_{\mathrm{I}} = 960$ nm, $\lambda_{\mathrm{II}} = 780$ nm, and $\lambda_{\mathrm{III}} = 690$ nm in the transmission spectra are denoted as modes I, II, and III, respectively. The different values of T_{+-}^{-z} and T_{-+}^{-z} lead to the AT effect, and the conversion efficiency under excited RCP light is larger than that under LCP light, giving the AT value a negative value. Figure 2(b) shows the AT spectrum of the OINs with the same structural parameters as those in Fig. 2(a). Three dips are observed around the three modes mentioned above.

To explore the AT mechanism on the OINs, the current and electric field distributions of the OINs at modes I, II, and III are shown in Fig. 3. The color represents the electric field strength. The magenta and gray arrows represent the electric current distributions. The yellow arrows represent the main electric current distributions of the OINs, and the equivalent magnetic dipole moments are labeled by $\vec{m}$. The different modes have been investigated by different section views, as shown in the bottom right corner of Fig. 3. Figure 3(a) shows the current and electric field distributions of mode I in the $x-y$ plane under LCP light excitation. A strong electric field is distributed in the gratings and tilted nanoslits. The circular current flows in the $x-y$ plane around the two terminals of the tilted nanoslits, which form two opposite equivalent magnetic dipoles $\vec{m}$ along the z axis. Hence, mode I attributes to the LSP resonances around the two terminals of the tilted nanoslits. A strong electric field is mainly distributed in the tilted nanoslits under RCP light excitation, whereas the current mode is the same as that under LCP light excitation, with the exception of $\vec{m}$ being in the opposite direction, as shown in Fig. 3(d). To obviously understand the results of AT, we calculated the electric field difference, $\Delta \boldsymbol{E} = \boldsymbol{E}_{\mathrm{LCP}} - \boldsymbol{E}_{\mathrm{RCP}}$, in Fig. 3(g), where $\Delta \boldsymbol{E}$ is the difference in electric field distribution between the LCP and RCP light excitations. The current and electric

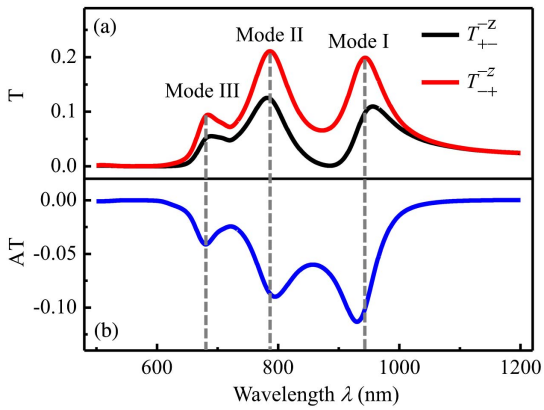

Fig. 2. (a) Transmission spectra of OIN arrays in the gold film under circularly polarized excitation along $-z$ direction. (b) AT spectrum of OIN arrays in the gold film. The three resonances are labeled modes I, II, and III.

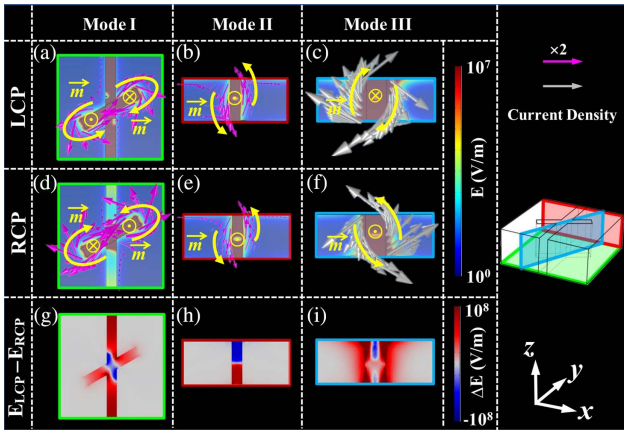

Fig. 3. Calculated current and electric field distributions of three modes of OIN arrays in the gold film under (a)–(c) LCP lights excitation and (d)–(f) RCP lights excitation. (g)–(i) show electric field difference $\boldsymbol{E}_{\mathrm{LCP}} - \boldsymbol{E}_{\mathrm{RCP}}$ of three modes, respectively. The current density of magenta arrows is two times larger than gray arrows. The map in the bottom right corner shows the section views of current and electric field distributions at different modes. The colors of picture frames of (a)–(i) are consistent with the colors of section views in the bottom right corner map.

distributions of mode II in the $x-z$ plane are shown in Figs. 3(b) and 3(e), respectively. A strong electric field is mainly distributed in the gratings. The spread of SPP from the top film surface to the gratings creates SPP resonance. Two equivalent magnetic dipoles $\vec{m}$ form along the y axis under different polarized lights. Although the directions of the two magnetic dipoles are the same, their magnitudes are different. Figure 3(h) shows that the electric field difference is mainly located in the gratings and has the opposite values in the upper and lower halves of gratings. In Figs. 3(c) and 3(f), the strong electric field of mode III is distributed in the tilted nanoslits. Due to the maximum electric field distribution, the section view of mode III is chosen as the bisector of the acute angle (β) between the gratings and tilted nanoslits. The spread of SPP from the top surface of the film to the tilted nanoslits generates the AT effect. The direction of equivalent magnetic dipole $\vec{m}$ is perpendicular to the section view of mode III. Meanwhile, the directions of $\vec{m}$ under LCP and RCP light excitations are opposite. In Fig. 3(i), the obvious difference in $\Delta\boldsymbol{E}$ is shown along the tilted nanoslits. Given the difference in refractive index between the resonance cavities of the nanoslits and the top surface of the OINs, the resonance wavelengths of modes II and III need to consider both the periods and thickness of the OINs. Mode II mainly attributes to the spread of SPP along the x direction on the top surface and in the gratings. The resonance wavelengths of mode II can be described as

$$\lambda_{\mathrm{II}} \propto n_{\mathrm{ts}} * P_x' + n_s * t', \tag{4}$$

where n_{ts} represents the effective refractive index of the top surface of the film, and n_s represents the effective refractive index of the nanoslits of the OINs. P_x', P_y', and t' represent the effective SPP oscillation length of the periods and thickness of the OINs. Mode III attributes to the spread of SPP on the top surface of the OINs and in the tilted nanoslits, which is closely

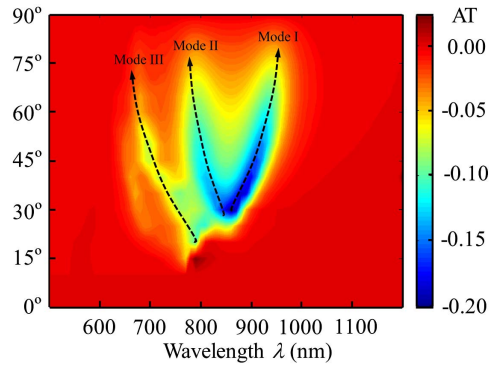

Fig. 4. Color map of AT values of OIN arrays in the gold film with angle β changed from 0° to 90°.

related to the periods in the x and y directions. Therefore, the resonance wavelengths of mode III can be described as

$$\lambda_{\mathrm{III}} \propto n_{\mathrm{ts}} * P_x' + n_{\mathrm{ts}} * P_y' + n_s * t'. \tag{5}$$

To investigate the influences of OIN structural parameters on the AT effect, Fig. 4 shows the color map of AT values when β changes from 0° to 90°. As a result of achiral structure, the AT value becomes zero when $\beta = 0°$ and $\beta = 90°$. The map obviously shows that mode I red shifts while modes II and III blue shift as β is increased from 0° to 90°. Mode I is formed by the circular LSP resonance at the two terminals of the tilted nanoslits. Thus, the effective magnetic dipole oscillation length increases with the increase in β, causing the red shift of mode I. Modes II and III result from the spread of SPP from the top surface of the OINs to the gratings and tilted nanoslits, respectively. The maximum areas of the gratings and tilted nanoslits in the $x-y$ plane are reached when $\beta = 90°$. The effective refractive index of the OINs decreases as the area decreases from $\beta = 0°$ to $\beta = 90°$ [33]. Hence, modes II and III blue shift as β increases. With both modes I and II resonating around the 870 nm wavelength, the absolute value of AT reaches its maximum when β is around 30°.

In addition, we sequentially investigate the influence of varied l, w, t, w_0, P_x, and P_y of OIN arrays on AT with other parameters fixed as in the control group. The AT spectra in Fig. 5(a) show that mode I red shifts while mode II almost keeps still, and mode III blue shifts as l is increased from

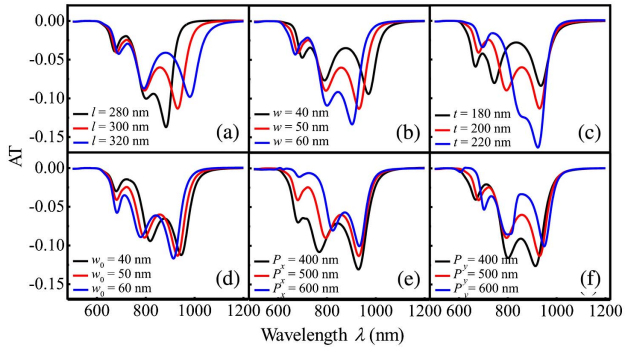

Fig. 5. Asymmetric transmission (AT) spectra of OIN arrays in the gold film with different (a) length l values, (b) width w values, (c) thickness t values, (d) width w_0 values, (e) period P_x values, and (f) period P_y values.

280 nm to 320 nm. With an increase in l, the effective magnetic dipole oscillation length increases, thereby resulting in the red shift of mode I. The SPP mainly spreads along z direction in the gratings of mode II, so the mode II does not shift as l increases. The increased l is equivalent to the narrowed tilted nanoslits, so the effective refractive index of tilted nanoslits increased [33]. Hence, mode III red shifts as l increases. On the contrary, in consideration of the aspect ratio of l and w, mode I blue shifts while mode II almost keeps still, and mode III red shifts as w increases, as shown in Fig. 5(b).

Figure 5(c) shows the AT spectra when t increases from 180 nm to 220 nm. Mode I blue shifts while mode II and III red shift as t increases. The LSP resonance of mode I is closely related to the resonance in the $x-y$ plane, so the increased t is equivalent to narrowed nanoslits in the $x-y$ plane. Thus, mode I blue shift as t increases. The increase of t increases the length of the resonant cavity, resulting in the red shift of mode II and mode III. As shown in Fig. 5(d), the w_0 is increased from 40 nm to 60 nm. Modes I and II blue shift, while mode III does not shift as w_0 increases. The increase of w_0 decreases the effective magnetic dipole oscillation length around the two terminals of tilted nanoslits, so mode I blue shifts as w_0 increases. Moreover, the effective refractive index of tilted nanoslits decreases when w_0 increases, causing the mode II blue shift. Given that mode III is principally attributed to SPP resonance along the z direction in the tilted nanoslits, the increase of w_0 does not affect SPP in tilted nanoslits, and mode III does not shift.

To investigate the effect of the period on the AT spectra, we vary the periods of the OIN arrays in the x and y directions. Due to the consideration of periods, the SPP spreads on the top surface of OINs coupled into the gratings and tilted nanoslits. In Figs. 5(e) and 5(f), mode I red shifts as P_x or P_y increases because of the increased effective magnetic dipole oscillation length. According to Eq. (4), the wavelengths of mode II red shift as P_x increases. Given that mode II formed mainly by SPP resonance in the gratings along z direction, and the gratings have infinite length, increased P_y has no effect on AT. In consequence, mode II almost does not shift as P_y increases, as Fig. 5(f) shows. According to Eq. (4), mode III red shifts as P_x or P_y increases, which attributes to the increased effective oscillation length of spreading SPP.

4. CONCLUSION

The AT property of OIN arrays under circularly polarized light excitation is studied using the finite element method. The transmission spectra, AT spectra, and charge distributions of the OINs are investigated to understand the AT mechanism. Three obvious dips appear in the AT spectrum because of the circular LSPs around the two terminals of the tilted nanoslits and the spread of SPP from the top surface of the OINs to the gratings or tilted nanoslits, respectively. The different responses in the OINs of RCP and LCP light excitations generate the AT effect, which strongly depends on the geometric parameters of the OINs. Therefore, the property of OINs not only contribute to elucidating the mechanism behind the AT effect but also to designing electromagnetic devices or polarization transformers.

Funding. National Natural Science Foundation of China (NSFC) (61575117); Fundamental Research Funds for the Central Universities (2016CSZ013); Ministry of Education of the People's Republic of China (GK201601008); Foundation for Excellent PhD Dissertation of Shaanxi Normal University (X2014YB08).

REFERENCES

1. A. B. Khanikaev, N. Arju, Z. Fan, D. Purtseladze, F. Lu, J. Lee, P. Sarriugarte, M. Schnell, R. Hillenbrand, M. A. Belkin, and G. Shvets, "Experimental demonstration of the microscopic origin of circular dichroism in two-dimensional metamaterials," Nat. Commun. **7**, 12045 (2016).
2. T. Fu, Y. Qu, G. Wang, Y. Wang, H. Li, J. Li, L. Wang, and Z. Zhang, "Tunable chiroptical response of chiral plasmonic nanostructures fabricated with chiral templates through oblique angle deposition," J. Phys. Chem. C **121**, 1299–1304 (2017).
3. Y. Wang, J. Deng, G. Wang, T. Fu, Y. Qu, and Z. Zhang, "Plasmonic chirality of L-shaped nanostructure composed of two slices with different thickness," Opt. Express **24**, 2307–2317 (2016).
4. S. Zhang, Y. S. Park, J. Li, X. Lu, W. Zhang, and X. Zhang, "Negative refractive index in chiral metamaterials," Phys. Rev. Lett. **102**, 023901 (2009).
5. B. Wang, J. Zhou, T. Koschny, and C. M. Soukoulis, "Nonplanar chiral metamaterials with negative index," Appl. Phys. Lett. **94**, 151112 (2009).
6. E. Plum, J. Zhou, J. Dong, V. A. Fedotov, T. Koschny, C. M. Soukoulis, and N. I. Zheludev, "Metamaterial with negative index due to chirality," Phys. Rev. B **79**, 035407 (2009).
7. C. Huang, Y. Feng, J. Zhao, Z. Wang, and T. Jiang, "Asymmetric electromagnetic wave transmission of linear polarization via polarization conversion through chiral metamaterial structures," Phys. Rev. B **85**, 195131 (2012).
8. C. Menzel, C. Helgert, C. Rockstuhl, E. B. Kley, A. Tünnermann, T. Pertsch, and F. Lederer, "Asymmetric transmission of linearly polarized light at optical metamaterials," Phys. Rev. Lett. **104**, 253902 (2010).
9. M. Mutlu, A. E. Akosman, A. E. Serebryannikov, and E. Ozbay, "Asymmetric transmission of linearly polarized waves and polarization angle dependent wave rotation using a chiral metamaterial," Opt. Express **19**, 14290–14299 (2011).
10. G. Kenanakis, A. Xomalis, A. Selimis, M. Vamvakaki, M. Farsari, M. Kafesaki, C. M. Soukoulis, and E. N. Economou, "Three-dimensional infrared metamaterial with asymmetric transmission," ACS Photon. **2**, 287–294 (2015).
11. V. A. Fedotov, P. L. Mladyonov, S. L. Prosvirnin, A. V. Rogacheva, Y. Chen, and N. I. Zheludev, "Asymmetric propagation of electromagnetic waves through a planar chiral structure," Phys. Rev. Lett. **97**, 167401 (2006).
12. E. Plum, V. A. Fedotov, and N. I. Zheludev, "Planar metamaterial with transmission and reflection that depend on the direction of incidence," Appl. Phys. Lett. **94**, 131901 (2009).
13. V. A. Fedotov, A. S. Schwanecke, N. I. Zheludev, V. V. Khardikov, and S. L. Prosvirnin, "Asymmetric transmission of light and enantiomerically sensitive plasmon resonance in planar chiral nanostructures," Nano Lett. **7**, 1996–1999 (2007).
14. J. Shi, X. Liu, S. Yu, T. Lv, Z. Zhu, H. Feng Ma, and T. Jun Cui, "Dual-band asymmetric transmission of linear polarization in bilayered chiral metamaterial," Appl. Phys. Lett. **102**, 191905 (2013).
15. Z. Wei, Y. Cao, Y. Fan, X. Yu, and H. Li, "Broadband polarization transformation via enhanced asymmetric transmission through arrays of twisted complementary split-ring resonators," Appl. Phys. Lett. **99**, 221907 (2011).
16. J. Han, H. Li, Y. Fan, Z. Wei, C. Wu, Y. Cao, X. Yu, F. Li, and Z. Wang, "An ultrathin twist-structure polarization transformer based on fish-scale metallic wires," Appl. Phys. Lett. **98**, 151908 (2011).
17. Z. Li, W. Liu, H. Cheng, S. Chen, and J. Tian, "Tunable dual-band asymmetric transmission for circularly polarized waves with

graphene planar chiral metasurfaces," Opt. Lett. **41**, 3142–3145 (2016).
18. J. Xu, P. Guan, P. Kvasnička, H. Gong, J. Homola, and Q. Yu, "Light transmission and surface-enhanced Raman scattering of quasi-3D plasmonic nanostructure arrays with deep and shallow Fabry-Perot nanocavities," J. Phys. Chem. C **115**, 10996–11002 (2011).
19. J. K. Gansel, M. Wegener, S. Burger, and S. Linden, "Gold helix photonic metamaterials: a numerical parameter study," Opt. Express **18**, 1059–1069 (2010).
20. J. K. Gansel, M. Latzel, A. Frölich, J. Kaschke, M. Thiel, and M. Wegener, "Tapered gold-helix metamaterials as improved circular polarizers," Appl. Phys. Lett. **100**, 101109 (2012).
21. L. Wu, Z. Yang, Y. Cheng, M. Zhao, R. Gong, Y. Zheng, J. Duan, and X. Yuan, "Giant asymmetric transmission of circular polarization in layer-by-layer chiral metamaterials," Appl. Phys. Lett. **103**, 021903 (2013).
22. M. Mutlu, A. E. Akosman, A. E. Serebryannikov, and E. Ozbay, "Asymmetric chiral metamaterial circular polarizer based on four U-shaped split ring resonators," Opt. Lett. **36**, 1653–1655 (2011).
23. C. Pfeiffer, C. Zhang, V. Ray, L. J. Guo, and A. Grbic, "High performance bianisotropic metasurfaces: asymmetric transmission of light," Phys. Rev. Lett. **113**, 023902 (2014).
24. H. Cao, J. Liang, X. Wu, Y. Pi, H. Xu, J. Liu, Z. Meng, and Y. Zhang, "Dual-band polarization conversion based on non-twisted Q-shaped metasurface," Opt. Commun. **370**, 311–318 (2016).
25. C. Pan, M. Ren, Q. Li, S. Fan, and J. Xu, "Broadband asymmetric transmission of optical waves from spiral plasmonic metamaterials," Appl. Phys. Lett. **104**, 121112 (2014).
26. R. Singh, E. Plum, C. Menzel, C. Rockstuhl, A. K. Azad, R. A. Cheville, F. Lederer, W. Zhang, and N. I. Zheludev, "Terahertz metamaterial with asymmetric transmission," Phys. Rev. B **80**, 153104 (2009).
27. A. S. Schwanecke, V. A. Fedotov, V. V. Khardikov, S. L. Prosvirnin, Y. Chen, and N. I. Zheludev, "Nanostructured metal film with asymmetric optical transmission," Nano Lett. **8**, 2940–2943 (2008).
28. Y. Wang, X. Wen, Y. Qu, T. Fu, and Z. Zhang, "Direct and indirect coupling mechanisms in a chiral plasmonic system," J. Phys. D **49**, 405104 (2016).
29. Y. Qu, X. Tian, T. Fu, G. Wang, G. Li, and Z. Zhang, "Broadband extraordinary optical transmission through a multilayer structure with a periodic nanoslit array," IEEE Photon. J. **7**, 1–8 (2015).
30. Z. Song and B. Zhang, "Wide-angle polarization-insensitive transparency of a continuous opaque metal film for near-infrared light," Opt. Express **22**, 6519–6525 (2014).
31. P. B. Johnson and R. W. Christy, "Optical constants of the noble metals," Phys. Rev. B **6**, 4370–4379 (1972).
32. Z. Li, M. Gokkavas, and E. Ozbay, "Manipulation of asymmetric transmission in planar chiral nanostructures by anisotropic loss," Adv. Opt. Mater. **1**, 482–488 (2013).
33. R. Zhou, H. Zhang, and H. Xin, "Metallic wire array as low-effective index of refraction medium for directive antenna application," IEEE Trans. Antennas Propag. **58**, 79–87 (2010).